

A chemical avenue to manipulate field-reentrant superconducting rivalries in infinite layer nickelates

Haowen Han^{1†}, Yusong Zhao^{1†}, Yi Bian¹, Wenlong Yang², Shaohua Yang³, Binghui Ge^{3*}, Hongliang Dong^{4,5}, Chuanying Xi⁶, Ze Wang⁶, Nuofu Chen⁷, Jia-Cai Nie^{2*}, Ho-kwang Mao^{4,5}, and Jikun Chen^{1*}

¹ *School of Materials Science and Engineering, University of Science and Technology Beijing, Beijing 100083, China.*

² *School of Physics and Astronomy, Beijing Normal University, Beijing 100875, China.*

³ *Institute of Physical Science and Information Technology, Anhui University, Anhui 230601, China.*

⁴ *Center for High Pressure Science and Technology Advanced Research, Shanghai 201203, China.*

⁵ *Shanghai Key Laboratory of Material Frontiers Research in Extreme Environments (MFree), Institute for Shanghai Advanced Research in Physical Sciences (SHARPS), Shanghai 201203, China.*

⁶ *Anhui Key Laboratory of Low-Energy Quantum Materials and Devices, High Magnetic Field Laboratory, HFIPS, Chinese Academy of Sciences, Hefei, Anhui 230031, China.*

⁷ *School of Renewable Energy, North China Electric Power University, Beijing 102206, China.*

[†] These authors contributed equally to this work

Abstract

Recently, a preliminary magnetic field-reentrant superconductivity manifested in high critical-temperature (T_c) Eu-doped infinite-layer (IL) nickelates¹⁻⁴, beyond analogous discoveries exclusively in low- T_c systems⁵⁻¹³. This arises more intriguing fundamental issues about potential quantum-phase boundary and criticality between unconventional superconductivity and field-reentrant-one, which are inexplicable owing to formidable challenges in growing IL-nickelates towards later-series rare-earths. Herein, we demonstrate the 4*f*-orbital related quantum rivalries between high- T_c and reentrant superconductivity in (Nd_{1-y}RE'_y)_{1-x}Eu_xNiO₂ (RE': Pr, Nd, Sm, Gd and Dy) system, via opening up the chemical avenue for a quantum leap in their growths. Robust magnetic field-reentrant superconductivity with uniaxial anisotropy is validated to fringe at boundary of the superconducting dome with optimal- T_c near 40 K. Reinforced reentry is realized via introducing Gd³⁺ with half-filled deeper 4*f*-orbital energy-states, compared to Eu²⁺, that strengthens on-site magnetic-moment. Our findings largely enrich the superconducting phase-diagram for nickelates, establishing an ideal platform for studying 4*f*-related unconventional superconductivity and quantum criticality.

Main

The participation of f -electrons in ferromagnetic coupling¹⁴, Kondo lattice^{14,15}, and antiferromagnetic exchange mediated Cooper-pairing^{16,17}, largely enriches the superconducting phase diagram also giving rise to magnetic field-reentrant superconductivity⁶. Recently, preliminary sign of reentrant superconductivity was observed via introducing the half-filled Eu^{2+} ($4f^7$) as hole dopant for infinite-layer (IL) nickelates^{2,4} that belongs to a new family of high temperature superconductor¹⁸ with T_c near ~ 40 K¹⁹. This is in stark contrast to the analogous earlier discoveries in exclusive low- T_c systems, such as UTe_2 ^{8,9}, URhGe ¹⁰, Eu-containing Chevrel phase compounds¹¹, λ -(BETS) $_2\text{FeCl}_4$ ¹² and moiré graphene¹³. It unveils a previously unexplored dimension associated with the $4f$ -orbital related rare-earth (RE) magnetism that may exert a substantial effect on superconducting phase diagram of nickelates, beyond their conventional ionic size effects^{20,21}. This observation further coincides with the distinct magnitude and anisotropy in the superconducting upper critical field as observed for IL nickelates with various magnetic contributions by the RE - $4f$ moments²². Also, it is more intriguing to note the generally elevated T_c of ambient pressured nickelate superconductor via substituting their RE composition towards later lanthanide series, as presently valid for not only IL nickelate^{1,19,22}, but also thin film layered perovskite nickelates²³⁻²⁶. In light of the prevailing trajectory of nickelate superconductors, venturing into heavier RE to map potential $4f$ -orbital effects on superconducting phase diagram offers the prospect of groundbreaking superconductivities and fundamental elucidations of underlying mechanisms.

Nevertheless, the key challenge in exploring nickelate superconductors towards heavier- RE lies in their material growths^{1,19,27}. Presently, successful growths of IL nickelates manifesting superconductivity were exclusively via vacuum epitaxy of perovskite nickelates precursors followed by topotactic reduction, limited to light- RE prior to Eu²⁸⁻³⁰. Unlike the existing IL-nickelates, introducing heavier RE (e.g., behind Eu) via vacuum deposition is thermodynamically obstructed, as their metastable perovskite nickelate precursor exhibits too positive formation free energy (ΔG) to be stabilized by a lattice coherent substrate^{31,32}. Owing to lanthanide contraction, declining the ionic radius of RE (r_{RE}) results in more distorted the NiO_6 octahedra within perovskite nickelates that exacerbates their positive ΔG ²⁰. Further obstacle is from the restriction in compositing the alkaline-earth (AE) hole dopants in 113-typed nickelates, since conventional chemical process is incapable to form Ni^{4+} in perovskites as major constituents even at extremely high p_{O_2} of $\sim \text{GPa}$ ^{21,33}. Thus, perovskite nickelates containing AE constituents were likely to be heterogeneously formed via plasma or atomic beam interplays with the substrate, contingent upon precise and narrowly defined experimental window^{1,19,27}. From these perspectives, the present strategy for growing infinite-layer nickelates is insufficient to support further explorations pertaining to heavier RE , despite its strong likelihood to realize higher T_c and/or unconventional superconductivity, e.g., field-reentry²⁻⁴.

Here, we open up the high- p_{O_2} chemical avenue for growing IL nickelate superconductors toward heavy- RE constituents with unprecedented effectiveness, grounded in which their $4f$ -

orbital relevant field-reentrant superconducting phase diagram is elucidated. The robust and uniaxially anisotropic superconducting reentrant behavior in $(\text{Nd}_{1-y}\text{RE}'_y)_{1-x}\text{Eu}_x\text{NiO}_2$ (RE' : Pr, Nd, Sm, Gd and Dy) systems is validated to fringed at quantum phase boundaries of the superconducting dome, showing optimal T_c near 40 K. The reentrant superconducting behavior is also tunable via RE^{3+} substitutions that alters the on-site magnetic moment associated with the 4*f*-orbital occupations and energy levels. Notably, the emergence of reentrant superconductivity is likely related to the suppression of superconductivity by other competing quantum states³⁴. This lays foundation to further study quantum criticality, unconventional superconductivity and their interactions^{7,35}, paving the way towards unveiling the mechanism behind high-temperature superconductivity. Also, a quantum leap in the growths of IL nickelates is realized via our chemical avenue, paving the way for their prospect applications as coated conductors analogous to cuprate high-temperature superconductors³⁶.

Enabling ultra-effective growths for IL-nickelates via high- p_{O_2} chemical avenue

From a thermodynamic perspective, the metastable perovskite nickelates precursors containing later series RE is more preferentially stabilized at a high- p_{O_2} within 10^0 - 10^2 MPa^{20,21,31}, as indicated by their equilibrium phase chart in Figure 1a. Thus, we exploit a MPa-high p_{O_2} assisted chemical strategy to more effectively reduce ΔG of perovskite nickelates, contracting with the lanthanide contraction. As illustrated in Extended Data Fig. 1, the perovskite nickelates was transformed into infinite layer via soft chemical topotactic reduction based on CaH_2 co-anneals. Instead of using conventional alkaline earth elements (e.g., Sr or Ca)^{37,38}, herein the hole doping was realized via partially substituting their RE -constituents by Eu, which displays variable valance state from +3 in perovskites towards +2 upon topotactic reduction¹. Compared to their state-of-the-art vacuum-based growth^{1,18,19,37}, our strategy is capable to introduce later series RE further behind Eu into IL-nickelates, while a high flexibility in adjusting RE is enabled by simply their chemical solutions for spin coating.

Efficient growth of IL-nickelates via our chemical route is exemplified for $\text{Nd}_{1-x}\text{Eu}_x\text{NiO}_2$ /substrate, covering a large variety of Eu compositions. The distinctive superiority for MPa-high p_{O_2} anneals in stabilizing metastable $\text{Nd}_{1-x}\text{Eu}_x\text{NiO}_3$ is indicated by their abrupt metal-insulator transition behaviors (see Figure 1b), as hardly achievable previously via vacuum depositions^{28,30,39}. Especially, the accuracy in the stoichiometry controls for Eu is convinced by the linear increase in critical temperatures (T_{MIT}) with x (or average r_{RE}), as in consistency with the previous reports for 113-typed perovskite nickelates^{20,21}, as shown by the inset of Figure 1b. More details in determination of T_{MIT} are shown in Extended Data Fig. 2. The X-ray diffraction patterns of as-grown $\text{Nd}_{0.55}\text{Eu}_{0.45}\text{NiO}_3$ demonstrate their oriented perovskite crystal structure, which transformed to the $\text{Nd}_{0.55}\text{Eu}_{0.45}\text{NiO}_2$ infinite layers after the topotactic reduction, while the results for more Eu-substituting compositions are shown in Supplementary Fig. 1. The resultant variation in electronic structure, e.g., from Ni^{3+} to Ni^{1+} , is further confirmed by synchrotron-based X-ray absorption spectroscopy (XAS) analysis, as results shown in Supplementary Fig. 2. Figure 1d shows the archetypal cross-section morphology for as-grown

$\text{Nd}_{1-x}\text{Eu}_x\text{NiO}_2$ / substrate as probed by high-angle annular dark-field (HAADF), where a larger thickness of ~ 15 nm is observed compared with the vacuum deposited ones (e.g., 6-8 nm)^{1,18,19,40}. It is also worth noticing that the $\text{Nd}_{1-x}\text{Eu}_x\text{NiO}_3$ percursor coherently grown on the substrate (see Supplementary Fig. 3), while the interfacial coherency was disrupted by the topotactic reduction, as a dead layer approaching to the interface is observed for $\text{Nd}_{1-x}\text{Eu}_x\text{NiO}_2$ /substrate.

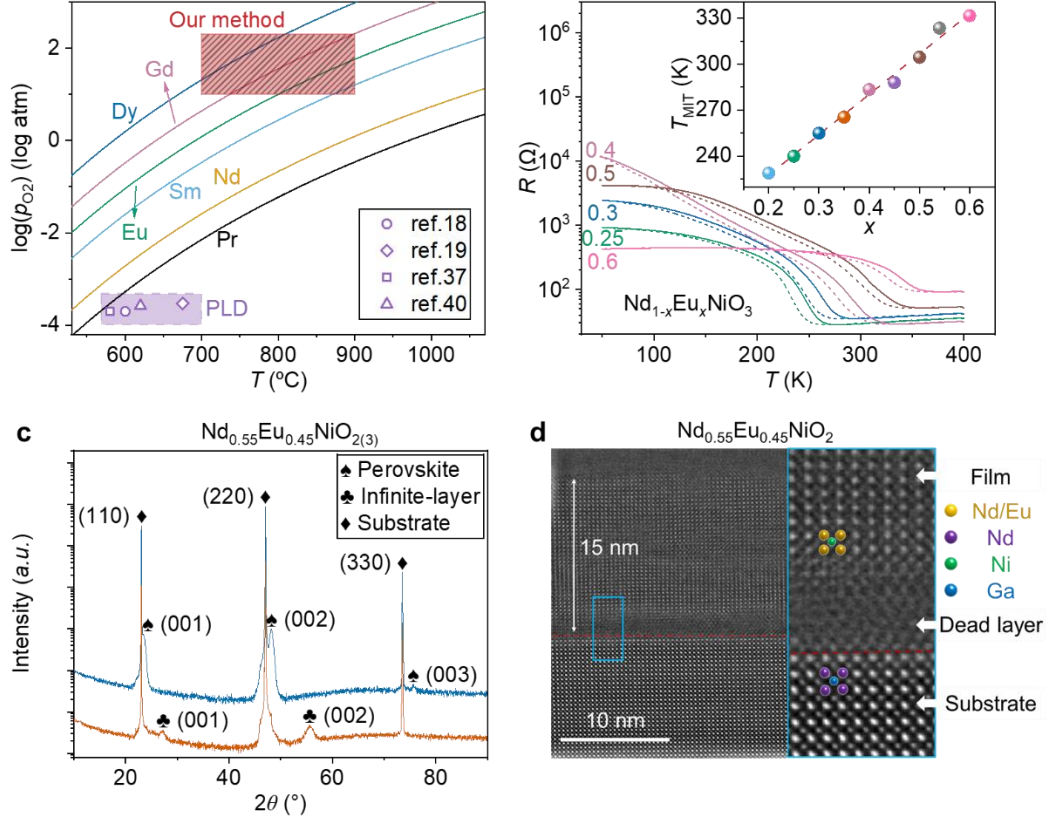


Fig. 1 | High oxygen pressure assisted chemical avenue for infinite-layer nickelates. **a**, The pressure-temperature (p - T) phase diagram for the formation of perovskite nickelates with different rare-earth elements under high oxygen pressure is depicted. The red region outlines the range of synthesis conditions encompassed by our method, with the slash area indicating the specific parameters employed in this work. The purple region, for comparison, represents the typical synthesis conditions for producing nickelate thin films via pulsed laser deposition (PLD)^{18,19,37,40}. **b**, Temperature dependence of resistance measured for $\text{Nd}_{1-x}\text{Eu}_x\text{NiO}_3$ thin films with various Eu-substituting compositions (x), convincing their abrupt metal-insulator transition behavior. The inset shows their critical temperature of MIT (T_{MIT}) versus x . **c**, The X-ray diffraction patterns for as-grown $\text{Nd}_{0.55}\text{Eu}_{0.45}\text{NiO}_3$ perovskite percursor and the $\text{Nd}_{0.55}\text{Eu}_{0.45}\text{NiO}_2$ infinite layer. **d**, Cross-sectional HAADF-STEM image of as-grown $\text{Nd}_{0.55}\text{Eu}_{0.45}\text{NiO}_2$ on substrate.

Expanded high- T_c superconducting dome with fringed reentry

Robust superconducting behaviors are observed for as-grown $\text{Nd}_{1-x}\text{Eu}_x\text{NiO}_2$ across a wide range of Eu substitutions (e.g., x : 0.25-0.55), with the highest $T_{c,\text{onset}}$ and $T_{c,\text{zero}}$ emerged at

optimum Eu constituents ($x=0.35-0.45$) reaching ~ 36 K and ~ 20 K, respectively. The temperature dependent resistances ($R-T$) of archetypal $\text{Nd}_{1-x}\text{Eu}_x\text{NiO}_2$ are shown in Figure 2a-2c for optimum doping ($x=0.45$), underdoping ($x=0.3$), and overdoping ($x=0.52$), respectively; while the $R-T$ tendencies for more Eu-doping constituents are provided in Extended Data Fig. 3. Within an optimum region of Eu-doping, the $\text{Nd}_{1-x}\text{Eu}_x\text{NiO}_2$ ($x=0.35-0.45$) manifests an expected superconducting state that is monotonically suppressed by magnetic fields up to 35 T, with no signature of reentrance down to 1.6 K. In stark contrast, a more intriguing magnetic field reentrant superconductivity is observed for both underdoped and overdoped $\text{Nd}_{1-x}\text{Eu}_x\text{NiO}_2$ (e.g., $x=0.3$ and 0.52), as demonstrated by their $R-B$ tendency in the insets of Figure 2b and 2c, respectively (see more results in Extended Data Fig. 4). At a low temperature (e.g., 2-3 K), the superconductivity firstly quenches at a low magnetic field of $\sim 1-2$ T, while further enlarging the magnetic field beyond 7-8 T results in reentrant superconductivity showing a zero resistance again. This observation is further evidenced by the crossing in their $R-T$ tendencies as measured under different magnetic fields (see Extended Data Fig. 5). It is worth noticing that the superconducting reentry in $\text{Nd}_{1-x}\text{Eu}_x\text{NiO}_2$ emerges exclusively at the superconducting boundaries, but is absent when the high- T_c superconductivity is robust with an optimum doping. This reveals the previously underestimated superconducting phase diagram with underlying quantum criticality associated with the on-site moment of $RE-4f^2$, giving rise to the likelihood of magnetic fluctuation enhanced pairing in the neighborhoods of quantum phase transitions⁷. The rivaling between reentrant and high- T_c superconductivities within $\text{Nd}_{1-x}\text{Eu}_x\text{NiO}_2$ is more clearly demonstrated by its superconducting phase diagram shown in Figure 2d. Of particular note is that the Eu in as-grown IL nickelates manifests a mixed valency between $+2$ and $+3$, the ratio of which was determined to be approximately $\text{Eu}^{3+}:\text{Eu}^{2+}=1:1$ from X-ray photoemission spectroscopy analysis as shown in Extended Data Fig. 6. Hence, about half of the Eu-composition (associated with Eu^{2+}) serves as the hole-dopant, and this is in consistency with the previous report on the same system¹. Accordingly, the hole doping range corresponding to the superconducting dome for our $\text{Nd}_{1-x}\text{Eu}_x\text{NiO}_2$ system is estimated to be within 0.1-0.3, which is similar to the $\text{Nd}_{1-x}\text{Sr}_x\text{NiO}_2$ ³⁷ as more clearly demonstrated in Extended Data Fig. 7.

Compared with the previous vacuum-based growth of $\text{Nd}_{1-x}\text{Eu}_x\text{NiO}_2$ ¹, our high- p_{O_2} chemical strategy better stabilizes Eu at high substituting compositions for mapping the superconducting phase diagram (Figure 2d), giving rise to a large elevation in T_c by $\sim 60\%$ at optimum doping. This further leads to the discovery of the rivaling superconducting reentrant states fringed at the quantum boundaries on both sides of the superconducting dome. In the underdoped region of the dome, the superconducting state has energy that is close to many competing states, such as charge order⁴¹, spin order³⁵ and/or oxygen order⁴². In the overdoped region near a hidden quantum critical point (QCP), where the system exhibits a transition from non-Fermi liquid (linear resistance) to Fermi liquid behavior³⁷, triggering a sudden change in electronic state. Near QCPs (indicated by the arrows in Extended Fig. 7), the magnetic fluctuations and the suppression of superconductivity by the competing quantum states⁴⁰ may lead to the reentrant superconductivity⁷.

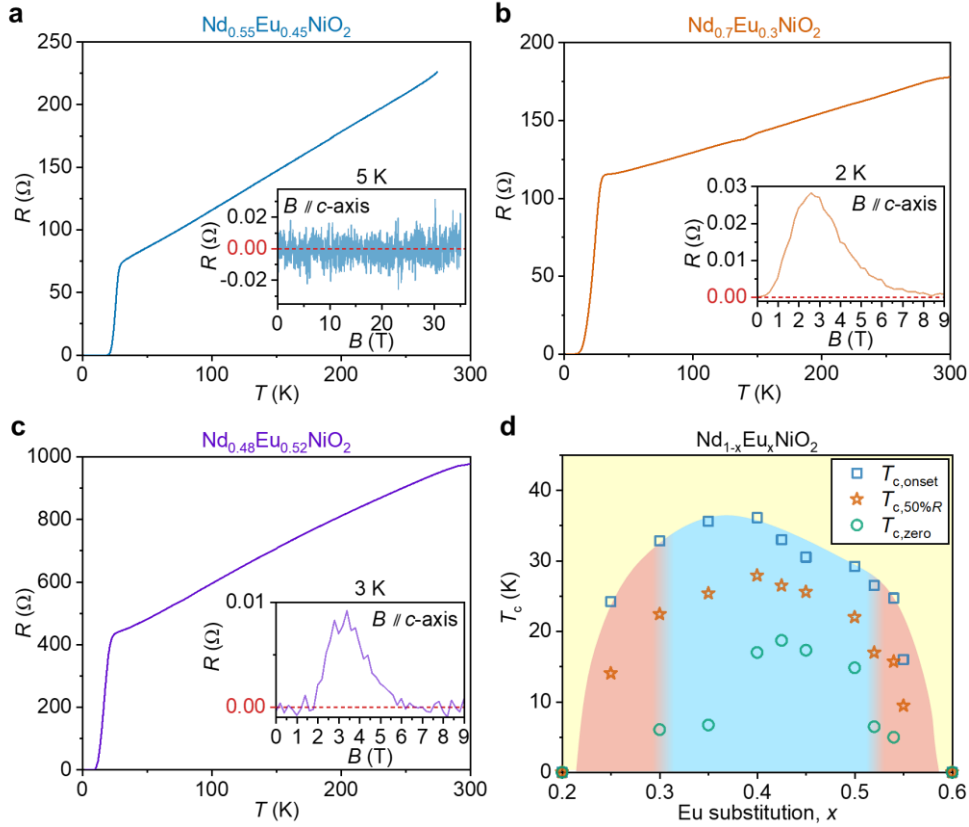


Fig. 2 | Discovery of field reentrant superconductivity fringed at quantum boundaries of superconducting dome. **a-c**, The temperature-dependent resistance (R - T) measured for: **a**, the optimally doped $\text{Nd}_{0.55}\text{Eu}_{0.45}\text{NiO}_2$, with the inset showing the corresponding magnetic field dependent resistance (R - B) at 5 K that demonstrated conventional superconductivity; **b**, the underdoped $\text{Nd}_{0.7}\text{Eu}_{0.3}\text{NiO}_2$, with the inset showing R - B at 2 K that demonstrates reentrance; **c**, overdoped $\text{Nd}_{0.48}\text{Eu}_{0.52}\text{NiO}_2$, with the inset showing R - B curve at 3 K that demonstrates reentrance. **d**, Superconducting phase diagram for $\text{Nd}_{1-x}\text{Eu}_x\text{NiO}_2$ plotted as a function of Eu substituting composition, x . The blue region represents the high- T_c superconducting region without reentry, while the red-shaded regions represent the emergence of magnetic field-reentrant superconductivity. The onset critical temperature ($T_{c,\text{onset}}$) is corresponding to the temperature where the electrical resistivity begins to deviate notably from its normal-state behavior. The midpoint transition temperature ($T_{c,50\%R}$) represents the temperature where the resistivity drops to 50% of its normal-state value (typically referenced to the value at $T_{c,\text{onset}}$). The zero-resistance temperature ($T_{c,\text{zero}}$) is defined as the temperature where the electrical resistivity drops below the experimental detection limit. The dome is established from samples at more Eu-substituting compositions, as shown by Extended Data Fig. 3.

Role of RE - $4f$ electrons in reentrant superconductivity

To elucidate the role of RE - $4f$ electrons in the reentrant superconductivity, we grew a series of $(\text{Nd}_{1-y}\text{RE}'_y)_{0.65}\text{Eu}_{0.35}\text{NiO}_2$ (RE' : Pr, Sm, Gd and Dy) to further modify the $4f$ -electron

configurates from $\text{Nd}_{0.65}\text{Eu}_{0.35}\text{NiO}_2$, which manifests only high- T_c superconductivity without reentry. The XRD patterns of as-grown $(\text{Nd}_{1-y}\text{RE}'_y)_{0.65}\text{Eu}_{0.35}\text{NiO}_3$ and $(\text{Nd}_{1-y}\text{RE}'_y)_{0.65}\text{Eu}_{0.35}\text{NiO}_2$ are shown in Supplementary Fig. 4, while the R - T tendencies of $(\text{Nd}_{1-y}\text{RE}'_y)_{0.65}\text{Eu}_{0.35}\text{NiO}_3$ are shown in Supplementary Fig. 5. Figure 3a shows the R - T tendencies for as-grown $(\text{Nd}_{0.9}\text{Pr}_{0.1})_{0.65}\text{Eu}_{0.35}\text{NiO}_2$, $(\text{Nd}_{0.9}\text{Sm}_{0.1})_{0.65}\text{Eu}_{0.35}\text{NiO}_2$, and $(\text{Nd}_{0.9}\text{Dy}_{0.1})_{0.65}\text{Eu}_{0.35}\text{NiO}_2$, where robust superconducting behaviors are observed, e.g., with $T_{c,\text{zero}}$ of ~ 20 K, 18 K and 14 K, respectively. As their R - B tendencies further demonstrated in the inset of Figure 4a and also Extended Data Fig. 8, these samples display no magnetic field reentrant behaviors. In contrast, the reentrant superconductivity emerges for $(\text{Nd}_{1-y}\text{Gd}_y)_{0.65}\text{Eu}_{0.35}\text{NiO}_2$ ($y=0.05, 0.1$ and 0.2) as demonstrated in Figure 3b and also the inset. Their R - B tendencies measured at more temperatures are further shown in Extended Data Fig. 8. Also, the Gd substitution results in lower $T_{c,\text{zero}}$ compared to the ones substituted by other RE . To further verify the magnetic field induced reentrant superconductivity, we measured their R - B tendencies up to higher magnetic fields at different temperatures, as archetypal results shown in Figure 3c for $\text{Nd}_{0.95}\text{Gd}_{0.05}\text{Eu}_{0.35}\text{NiO}_2$. It clearly demonstrates the emergence of superconducting reentries reaching zero resistances from 5-10 T, 8-13 T and 10-15 T at 1.6 K, 2 K, and 3 K, respectively, further quenching at 30 T, 25 T and 20 T.

The distinct superconducting behavior in $(\text{Nd}_{1-y}\text{RE}'_y)_{0.65}\text{Eu}_{0.35}\text{NiO}_2$ at various RE assist in understanding the root cause for the reentrant superconductivity within IL-nickelates and its struggle for primacy with the previously observed high- T_c superconductivity. Among the lanthanide rare-earth ions, both the Eu^{2+} and Gd^{3+} exhibit a half filled $4f$ -shell (e.g., $4f^7$, $J=7/2$), contributing a large effective moment ($\mu_{\text{eff}} \approx 7 \mu_B$)⁴³. Thus, introducing Eu^{2+} or Gd^{3+} within IL-nickelates would effectively strengthen the on-site moment, allowing their further interplays with carriers and/or their Cooper-pairing⁴⁴ to enrich the superconducting phase diagram. Nevertheless, the Eu^{2+} $4f$ -orbital usually contributes a shallower energy level, compared to Gd^{3+} $4f$ -orbital, when forming the valance band in oxides⁴⁵. This elevates the likelihood of exchange interactions between $4f$ -related ferromagnetic moments and d -orbital dominated conduction band, as responsible for the ferromagnetic phase transition observed in EuO ⁴⁴. In contrast, the $4f$ -orbital from Gd^{3+} forms deeper valance energy level that is unlikely to arise analogous d -orbital interplays. This may count for the striking dichotomy when substituting $\text{Nd}_{0.65}\text{Eu}_{0.35}\text{NiO}_2$ slightly via Gd^{3+} or Eu^{2+} : the superconducting reentry emerges in the former scenario, while for the latter case the conventional superconductivity further strengthened. Multiple mechanisms responsible for the magnetic field induced reentrant superconductivity were proposed, such as spin-triplet pairing⁹, metamagnetic criticality⁴⁶ and Jaccarino-Peter effect^{47,48}. In sight of the deeper $4f^7$ -orbital electrons in Gd^{3+} , the reentrant superconductivity is more likely relevant to Jaccarino-Peter compensation mechanism, in which situation the Gd^{3+} substituent can strengthen the on-site moment. Consequently, an internal exchange field (H_J) is generated to partially against the externally magnetic field (H_{ext}), reducing its resultant pair-breaking for superconducting reentry as illustrated in Figure 3d²⁻⁴.

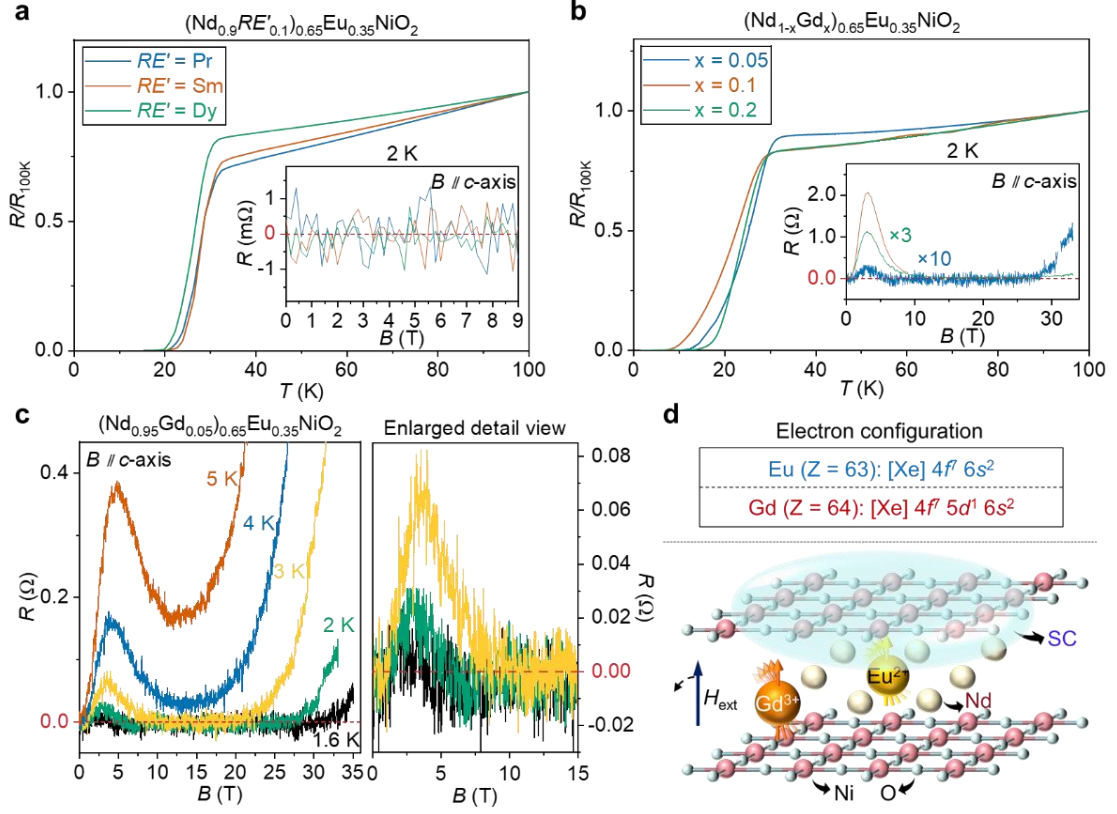


Fig. 3 | Further modification in field-reentrant superconductivity via introducing more rare-earth substituents. **a**, The normalized temperature dependent resistance ($R-T$) measured for $(Nd_{0.9}RE'_{0.1})_{0.65}Eu_{0.35}NiO_2$ ($RE' = Pr, Sm$ and Dy), displaying robust conventional superconductivity. The inset shows their corresponding magnetic field dependent resistance ($R-B$) measured at 2 K. **b**, The normalized $R-T$ as measured for $(Nd_{1-y}Gd_y)_{0.65}Eu_{0.35}NiO_2$ ($y = 0.05, 0.1$ and 0.2), showing clear field-reentrant superconductivity. The inset shows their corresponding $R-B$ measured at 2 K. **c**, $R-B$ measurements of $(Nd_{0.95}Gd_{0.05})_{0.65}Eu_{0.35}NiO_2$ up to higher magnetic fields at different temperature. **d**, Schematic illustration of the proposed mechanism: the $4f^7$ moments of Gd^{3+} located at deeper energy level generate an internal exchange field (H_i) that partially compensates the external magnetic field (H_{ext}) via the Jaccarino-Peter effect⁴⁷, giving rise to reentrant superconductivity.

Anisotropy in filed reentrant superconductivity

Open question further raises associated with the potential anisotropy in the above observed reentrant superconductivity, which is the case for previously discovered reentrant systems, such as UTe_2 ⁶. To elucidate this issue, we performed angular dependent magneto-transport measurements via systematically altering the cross-plane angle between H_{ext} and the norm (θ), e.g., $\theta = 0^\circ$ and 90° representing for H_{ext} parallels to c -axis and ab -plane, respectively. Figure 4 shows the resistance of $(Nd_{0.95}Gd_{0.05})_{0.65}Eu_{0.35}NiO_2$ mapped as a function of both magnetic field strength and θ at various temperatures of 2 K, 3 K, 5 K and 10 K. The magnitudes of resistance were acquired from their $R-B$ tendencies as measured at each θ (see Extended Data Fig. 9) and demonstrated by a color scale, e.g., deep blue indicating vanishing resistance (superconducting

state), while gradual reddish color change signifying elevation in resistance. More distinctly separated regions associated with the low magnetic field (e.g., $H_{\text{ext}} < 10$ T) and the field reentrant (e.g. H_{ext} of ~ 26 T) superconductivity are observed when imparting H_{ext} along c -axis (θ approaching to 0°). Also, elevating the temperature (e.g., from 2 K to 5 K) results in markedly contraction in the reentrant region. Similar phenomenon was also observed for other compositions, as further shown in Extended Data Fig. 10. These angular and temperature dependent resistive mapping demonstrates strong uniaxial *cross-plane* anisotropy in the superconducting reentrant behavior of IL-nickelates, as preferentially emerging at low temperatures.

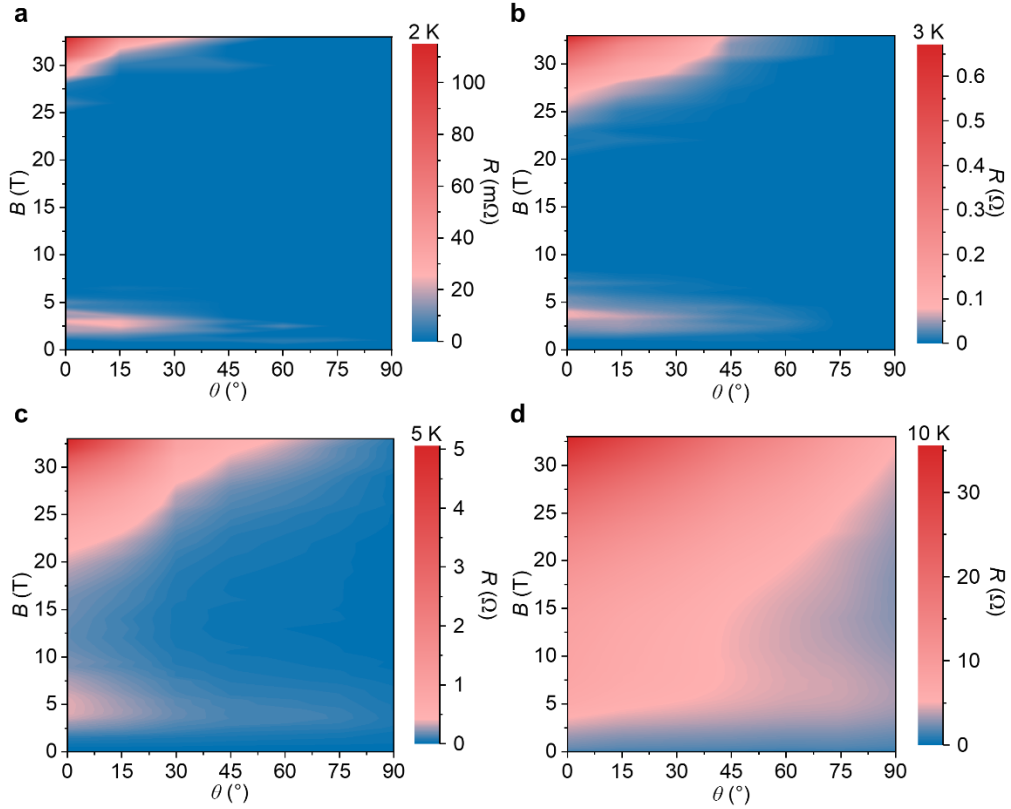


Fig. 4 | Uniaxial anisotropy of field-reentrant superconductivity revealed by angular magneto-transport at various temperatures. a-d, Resistance mapping of $(\text{Nd}_{0.95}\text{Gd}_{0.05})_{0.65}\text{Eu}_{0.35}\text{NiO}_2$ at: **a**, 2 K; **b**, 3 K; **c**, 5 K; and **d**, 10 K. The deep blue regions of zero resistance (reentrant superconductivity) emerging at high fields when H_{ext} is near the c -axis ($\theta \approx 0^\circ$), revealing strong uniaxial anisotropy, while elevating the temperature progressively suppresses the reentrant superconducting phase, constraining it to a narrower range of angles and fields.

Taken together the high anisotropy of reentrant superconductivity and the distinct $4f$ -orbital interplays from Eu^{2+} compared to Gd^{3+} , it unveils the complication in underneath mechanism associated with the reentrant superconductivity for $(\text{Nd}_{1-y}\text{RE}'_y)_{1-x}\text{Eu}_x\text{NiO}_2$ system. Although the Jaccarino-Peter compensation effect may explain the strengthened reentry via Gd^{3+} substitutions, it is less likely to completely rule out other mechanisms, e.g., spin-triplet

pairing enhanced by magnetic fluctuations⁶ or metamagnetic criticality accompanied by Fermi surface reconstruction⁴⁶. It is worth noticing that the exchange induced rivelling between singlet and triplite state of electron pairs attract by oxygen vacancy well explains the anomalously abrupt ferromagnetic metal-insulator transition of EuO⁴⁴. Considering the highly probable emergence of oxygen vacancy within IL nickelates during topotactic reductions, it sheds a light on analogous transition between singlet and triplite state of electron paring that may also related to superconducting reentry.

Outlook

In summary, we discover the rivalling field-reentrant superconducting states that fringed at the two quantum boundaries of the superconducting dome peaked at $T_c=36$ K in Eu-doped infinite-layer nickelate system, via enabling their ultra-effective growths grounded in a high- pO_2 chemical avenue. Angular and temperature dependent magneto-transport measurements convinced the uniaxial anisotropic nature of the reentrant superconductivity that is preferentially emerged at low temperatures. The reentry arises from magnetic fluctuations near QCPs and the suppression of superconductivity by other competing quantum states, and was further strengthened via enlarging the on-site moment, e.g., when introducing Gd^{3+} with half-filled 4*f*-orbital located at deeper energy level compared to Eu^{2+} . We highlight the overlooked 4*f*-related orbital interplays and magnetic moments that further complicate the superconducting phase diagram of IL-nickelates, beyond analogous cuprates with similar *d*-orbital frameworks. Thus, it provides a new freedom for regulating superconducting pairing strength, and also establishes ideal platforms for studying quantum criticality, unconventional superconductivity and their interactions. Furthermore, the non-vacuum incoherently growth of IL nickelate with high effectiveness holds significant practical implications, particularly in its potential to leverage coated conductor technologies similar to those presently used in cuprates enabling scalable production.

Competing interests: We declare no competing financial interest.

Additional information: Supplementary Information is available for this manuscript.

Correspondences: Correspondence should be addressed: Prof. Jikun Chen (jikunchen@ustb.edu.cn), Prof. Jia-Cai Nie (jcnie@bnu.edu.cn) and Prof. Binghui Ge (bhge@ahu.edu.cn).

Author contributions: J.C. and J.N. conceived the project. H.H. and Y.Z. contributed equally to this work. H.H. performed the soft chemical reduction experiments, transport measurements, and XRD characterizations. Y.Z. synthesized the perovskite precursor films assisted by N.C. Y.B. and W.Y. assisted in the transport measurements. H.H., C.X., and Z.W. performed the high-field magneto-transport measurements. S.Y. and B.G. conducted the STEM experiments. H.D performed the XAS experiments assisted by K.M. J.C, J.N. B.G, N.C and

K.M provided constructive experimental supports and discussions. All authors analysed and discussed the data. J.C. wrote the manuscript, assisted by H.H. and J.N, also with input from all authors.

Acknowledgments: This work was supported the National Key Research and Development Program of China (No. 2021YFA0718900), the National Natural Science Foundation of China (No. 92065110 and 12474001). We thank the BL08U1A beamline and the User Experiment Assist System of the Shanghai Synchrotron Radiation Facility (SSRF) for the assistance in characterizations. We also thank the staff members of the XMCD beamline at the NSRL in Hefei, for providing the technical support and assistance in XAS data collection and analysis. We also thank the WM1 of the Steady High Magnetic Field Facility, Chinese Academy of Sciences, for the assistance on the experiment.

References

- 1 Wei, W., Vu, D., Zhang, Z., Walker, F. J. & Ahn, C. H. Superconducting $\text{Nd}_{1-x}\text{Eu}_x\text{NiO}_2$ thin films using in situ synthesis. *Sci Adv* **9**, eadh3327 (2023).
- 2 Yang, M. *et al.* Robust field re-entrant superconductivity in ferromagnetic infinite-layer rare-earth nickelates. *arXiv 2508.14666* (2025).
- 3 Vu, D. *et al.* Unconventional superconductivity induced by rare-earth substitution in $\text{Nd}_{1-x}\text{Eu}_x\text{NiO}_2$ thin films. *arXiv 2508.15968* (2025).
- 4 Rubi, K. *et al.* Extreme magnetic field-boosted superconductivity in a high-temperature superconductor. *arXiv 2508.16290* (2025).
- 5 Meul, H. W. *et al.* Observation of Magnetic-Field-Induced Superconductivity. *Physical Review Letters* **53**, 497-500 (1984).
- 6 Ran, S. *et al.* Extreme magnetic field-boosted superconductivity. *Nature physics* **15**, 1250-1254 (2019).
- 7 Ran, S. *et al.* Nearly ferromagnetic spin-triplet superconductivity. *Science* **365**, 684-687 (2019).
- 8 Lewin, S. K. *et al.* High-field superconducting halo in UTe_2 . *Science* **389**, 512-515 (2025).
- 9 Ran, S. *et al.* Nearly ferromagnetic spin-triplet superconductivity. *Science* **365**, 684-687 (2019).
- 10 Lévy, F., Sheikin, I., Grenier, B. & Huxley, A. D. Magnetic Field-Induced Superconductivity in the Ferromagnet URhGe. *Science* **309**, 1343-1346 (2005).
- 11 Burlet, P. *et al.* Magnetism and superconductivity in the Chevrel phase HoMo_6S_8 . *Physica B: Condensed Matter* **215**, 127-133 (1995).
- 12 Uji, S. *et al.* Magnetic-field-induced superconductivity in a two-dimensional organic conductor. *Nature* **410**, 908-910 (2001).
- 13 Cao, Y., Park, J. M., Watanabe, K., Taniguchi, T. & Jarillo-Herrero, P. Pauli-limit violation and re-entrant superconductivity in moiré graphene. *Nature* **595**, 526-531 (2021).
- 14 Shen, B. *et al.* Strange-metal behaviour in a pure ferromagnetic Kondo lattice. *Nature* **579**, 51-55 (2020).
- 15 Iglesias, J. R., Lacroix, C. & Coqblin, B. Revisited Doniach diagram: Influence of short-range antiferromagnetic correlations in the Kondo lattice. *Physical Review B* **56**, 11820 (1997).

- 16 Araki, S., Nakashima, M., Settai, R., Kobayashi, T. C. & Onuki, Y. Pressure-induced superconductivity in an antiferromagnet CeRh₂Si₂. *Journal of Physics: Condensed Matter* **14**, L377 (2002).
- 17 Mathur, N. *et al.* Magnetically mediated superconductivity in heavy fermion compounds. *Nature* **394**, 39-43 (1998).
- 18 Li, D. *et al.* Superconductivity in an infinite-layer nickelate. *Nature* **572**, 624-627 (2019).
- 19 Chow, S. L. E., Luo, Z. & Ariando, A. Bulk superconductivity near 40 K in hole-doped SmNiO₂ at ambient pressure. *Nature* **642**, 58-63 (2025).
- 20 Chen, J. *et al.* Overcoming synthetic metastabilities and revealing metal-to-insulator transition & thermistor bi-functionalities for d-band correlation perovskite nickelates. *Materials Horizons* **6**, 788-795 (2019).
- 21 Alonso, J. A., Martínez-Lope, M. J., Casais, M. T., Aranda, M. A. G. & Fernández-Díaz, M. T. Metal–Insulator Transitions, Structural and Microstructural Evolution of RNiO₃ (R = Sm, Eu, Gd, Dy, Ho, Y) Perovskites: Evidence for Room-Temperature Charge Disproportionation in Monoclinic HoNiO₃ and YNiO₃. *Journal of the American Chemical Society* **121**, 4754-4762 (1999).
- 22 Wang, B. Y. *et al.* Effects of rare-earth magnetism on the superconducting upper critical field in infinite-layer nickelates. *Science advances* **9**, eadf6655 (2023).
- 23 Zhou, G. *et al.* Ambient-pressure superconductivity onset above 40 K in (La, Pr)₃Ni₂O₇ films. *Nature* **640**, 641-646 (2025).
- 24 Liu, Y. *et al.* Superconductivity and normal-state transport in compressively strained La₂PrNi₂O₇ thin films. *Nature Materials*, 1-7 (2025).
- 25 Hao, B. *et al.* Superconductivity in Sr-doped La₃Ni₂O₇ thin films. *Nature Materials*, 1-7 (2025).
- 26 Ji, H. *et al.* Signatures of spin-glass superconductivity in nickelate (La, Pr, Sm)₃Ni₂O₇ films. *arXiv 2508.16412* (2025).
- 27 Yang, M. *et al.* Enhanced superconductivity in co-doped infinite-layer samarium nickelate thin films. *arXiv 2503.18346* (2025).
- 28 Chen, J. *et al.* Electron-Doping Mottronics in Strongly Correlated Perovskite. *Advanced Materials* **32**, 1905060 (2020).
- 29 Zhang, H.-T. *et al.* Reconfigurable perovskite nickelate electronics for artificial intelligence. *Science* **375**, 533-539 (2022).
- 30 Zhang, Z. *et al.* Perovskite nickelates as electric-field sensors in salt water. *Nature* **553**, 68-72 (2018).
- 31 Chen, J. *et al.* Pressure Induced Unstable Electronic States upon Correlated Nickelates Metastable Perovskites as Batch Synthesized via Heterogeneous Nucleation. *Advanced Functional Materials* **30**, 2000987 (2020).
- 32 Jaramillo, R., Schoofs, F., Ha, S. D. & Ramanathan, S. High pressure synthesis of SmNiO₃ thin films and implications for thermodynamics of the nickelates. *Journal of Materials Chemistry C* **1**, 2455-2462 (2013).
- 33 Ye, X. *et al.* High-temperature ferrimagnetic order triggered metal-to-insulator transition in CaCu₃Ni₂Os₂O₁₂. *Nature Communications* **16**, 3746 (2025).
- 34 Sun, L. *et al.* Re-emerging superconductivity at 48 kelvin in iron chalcogenides. *Nature* **483**, 67-69 (2012).

- 35 Keimer, B., Kivelson, S. A., Norman, M. R., Uchida, S. & Zaanen, J. From quantum matter to high-temperature superconductivity in copper oxides. *Nature* **518**, 179-186 (2015).
- 36 MacManus-Driscoll, J. L. & Wimbush, S. C. Processing and application of high-temperature superconducting coated conductors. *Nature Reviews Materials* **6**, 587-604 (2021).
- 37 Lee, K. *et al.* Linear-in-temperature resistivity for optimally superconducting (Nd, Sr) NiO₂. *Nature* **619**, 288-292 (2023).
- 38 Zeng, S. *et al.* Superconductivity in infinite-layer nickelate La_{1-x}Ca_xNiO₂ thin films. *Science advances* **8**, eabl9927 (2022).
- 39 Shi, J., Zhou, Y. & Ramanathan, S. Colossal resistance switching and band gap modulation in a perovskite nickelate by electron doping. *Nature Communications* **5**, 4860 (2014).
- 40 Sahib, H. *et al.* Superconductivity in PrNiO₂ Infinite-Layer Nickelates. *Advanced Materials* **37**, 2416187 (2025).
- 41 Fernandes, R. M. *et al.* Iron pnictides and chalcogenides: a new paradigm for superconductivity. *Nature* **601**, 35-44 (2022).
- 42 Parzyck, C. T. *et al.* Absence of 3a₀ charge density wave order in the infinite-layer nickelate NdNiO₂. *Nature materials* **23**, 486-491 (2024).
- 43 Zhang, H. *et al.* High-mobility spin-polarized two-dimensional electron gases at EuO/KTaO₃ interfaces. *Physical review letters* **121**, 116803 (2018).
- 44 Petrich, G., Von Molnár, S. & Penney, T. Exchange-induced autoionization in Eu-rich EuO. *Physical Review Letters* **26**, 885 (1971).
- 45 Shai, D. E. *et al.* Temperature Dependence of the Electronic Structure and Fermi-Surface Reconstruction of Eu_{1-x}Gd_xO through the Ferromagnetic Metal-Insulator Transition. *Physical Review Letters* **108**, 267003 (2012).
- 46 Wu, Z. *et al.* A quantum critical line bounds the high field metamagnetic transition surface in UTe₂. *Physical Review X* **15**, 021019 (2025).
- 47 Jaccarino, V. & Peter, M. Ultra-high-field superconductivity. *Physical Review Letters* **9**, 290 (1962).
- 48 Helm, T. *et al.* Field-induced compensation of magnetic exchange as the possible origin of reentrant superconductivity in UTe₂. *Nature Communications* **15**, 37 (2024).